An Eulerian Model of Dispersion in the Convective Boundary Layer Using Explicit Periodic Advections

JOHN J. CARROLL AND MING LIU

Department of Land, Air, and Water Resources, University of California at Davis, Davis, California

(Manuscript received 8 October 1994, in final form 1 May 1995)

ABSTRACT

The authors have developed a relatively simple, first-order closure, Eulerian diffusion model, in which turbulent coherent structures of the convective boundary layer are explicitly included as periodic velocities imposed on a stationary and horizontally homogeneous wind field. The dimensions of the convective updrafts and downdrafts are assumed to be inversely proportional to the ratio of their respective vertical speeds and are constant with height, and the updraft and downdraft areas are constant in the horizontal. Sinusoidal vertical velocity variations are specified with amplitudes proportional to the mean vertical velocity profiles for skewed distributions described by Weil. The horizontal velocity components of the coherent structures are calculated using the continuity equation. Model simulations for conditions on the afternoon of Wangara day 33 reproduce the major features of the complicated plume dispersion behavior observed in the water tank experiments and the CONDORS experiments. The model produces results comparable to those obtained by complex large-eddy simulation models and random walk Lagrangian models, but is computationally much less demanding. Sensitivity tests are presented that show that the model is insensitive to physically realistic ranges of the modeling parameters.

1. Introduction

The traditional view, that turbulence in the atmospheric boundary layer is composed of an ensemble of random, diffusive, and chaotic eddies, is becoming replaced by the recognition that coherent structures are an inherent part of these flows and play a very large role in the "diffusion" of mass and energy within the boundary layer (Schmidt and Schumann 1989; Gao et al. 1989; Shaw et al. 1989; Robinson 1991). For very unstable conditions, the existence of convective plumes intermittently transporting fluid vertically from one boundary to the other is well recognized (e.g., Webb 1964; Kaimal et al. 1976; Hunt et al. 1988; Quintarelli 1990; Huynh et al. 1990). The effects of these convective plumes on the dispersion of material emitted into the convective boundary layer (CBL) have been studied in the laboratory experiments of Willis and Deardorff (1976, 1978, 1981, hereafter WD), which comprise the standard cases against which dispersion models are tested, and in the CONDORS field experiments (Briggs 1993).

Planetary boundary layer (PBL) models that use varying degrees of turbulence closure fail to reproduce observed dispersion properties of the CBL, especially the well-mixed condition of the middle 80% of the CBL (e.g., Mellor and Yamada 1974, 1982; Carroll 1993). Even the complex third-order closure model of Andre et al. (1978) was not fully successful in this regard. Alternative modeling techniques, such as direct turbulence simulation (Enger 1986) and large-eddy simulation (Deardorff 1974; Moeng 1984; Schmidt and Schumann 1989; Nieuwstadt and de Valk 1987), do better but have very high computational demands. Dispersion in the CBL has been extensively explored using stochastic Lagrangian models to simulate the combined effects of the background wind and the "dominant" eddies on pollutant dispersion (Lamb 1982; Reid 1979; Baerentsen and Berkowicz 1984; de Baas et al. 1986; Sawford and Guest 1987; Thomson 1987; Luhar and Britter 1989; Weil 1990; Hurley and Physick 1993). The more recent of these include skewed vertical velocity distributions and have been successful in reproducing the major features of the WD experiments.

We propose a different approach in which the coherent structures, in this case the convective plumes, are included explicitly as advective velocities in an Eulerian model with first-order closure parameterization for the diffusive effects of incoherent turbulence. We use the properties of the convective motions, as observed and as formulated for Lagrangian random walk models, as functions of the stability to define coherent structures that are periodic in the horizontal. The succession of convective plumes, so defined, is then advected through the computational domain, producing temporally periodic variation of the local velocity

Corresponding author address: Dr. John J. Carroll, Department of Land, Air, and Water Resources, University of California at Davis, Hoagland Hall, Davis, CA 95616-8627.
E-mail: carroll@atm1.ucdavis.edu

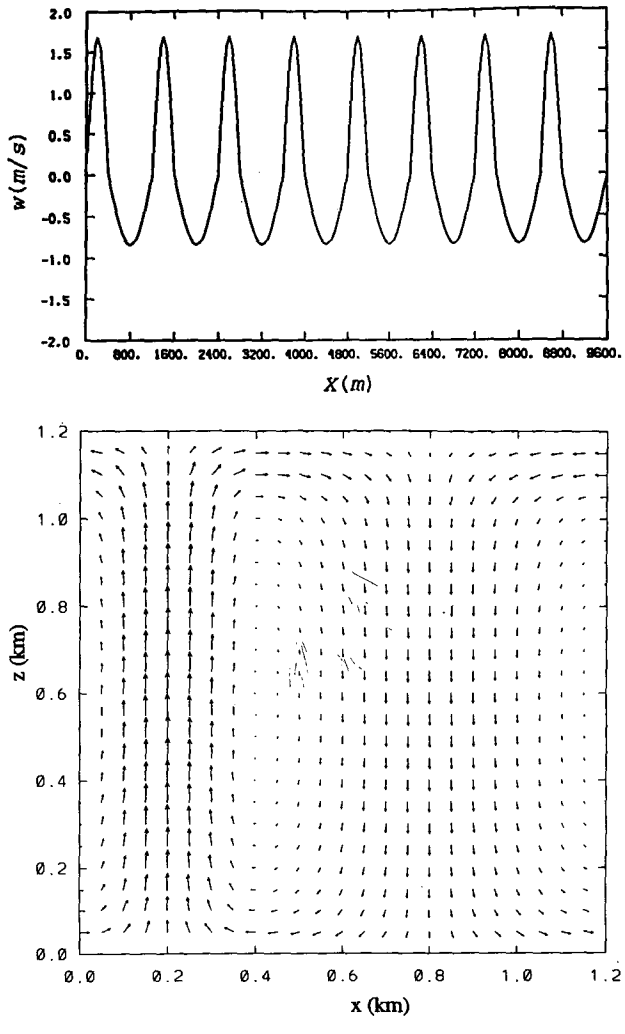

FIG. 1. (a) Instantaneous view of the horizontal variation of w at $0.5z_i$. (b) Instantaneous view of the perturbation velocity vector in an x–z plane for one pair of up- and downdrafts.

components and their advections. Our approach is similar to the two-stream model of Chatfield and Brost (1987) but differs in the plume geometry, in our use of two-dimensional space, and in our explicit calculation of horizontal divergence associated with convective plumes.

For the purposes of this discussion, the stability conditions, the vertical profile of the mean wind, and the statistical properties of the flow are assumed constant in time and in the horizontal. These conditions, profiles, and properties can be prescribed from observations or from boundary layer model simulations. Our purpose here is to explore the concept of an explicit periodic advection model and its sensitivity to modeling assumptions.

2. Formulation

We assume the horizontal wind has no directional variation with height, the x axis is aligned in the downwind direction, and advection in the downwind direction greatly exceeds downwind diffusion. We also assume vertical advection is caused by convective plumes only; that is, the long-term mean vertical velocity is zero. To be consistent with previous modeling conventions and the WD experiments, we ignore crosswind diffusion and transport variations, that is, focus on the crosswind-integrated concentration C_y. With these simplifications, the local variation in the concentration C_y of an inert, conservative material can be written as

$$\frac{\partial C_y}{\partial t} = -(U+u)\frac{\partial C_y}{\partial x} - w\frac{\partial C_y}{\partial z} - \frac{\partial}{\partial z}\left(-K_h\frac{\partial C_y}{\partial z}\right). \tag{1}$$

Here U is the horizontal mean wind, a function of z only, and u and w are the resolvable horizontal and vertical components of the coherent structure flow elements and are both functions of x, z, and t. The concentration C_y is an average over the diffusive timescale but varies as a result of the slower periodic advection. The relationship between u and w is the incompressible conservation of mass:

$$\frac{\partial u}{\partial x} + \frac{\partial w}{\partial z} = 0 \tag{2}$$

or

$$u(x,t) = -\int \frac{\partial w}{\partial z}\,dx. \tag{3}$$

In (1), K_h is vertical eddy diffusivity, and the last term is the parameterization of subgrid-scale turbulent fluxes.

For the CBL, vertical profiles of the standard deviation and third moment of w are available from observations (Lenschow et al. 1980; Kaimal et al. 1976) and from large-eddy simulation model outputs (e.g., Moeng and Wyngaard 1984, 1989). Based on these, Weil (1990) suggests the following profiles for the turbulence statistics:

$$\sigma_w(z) = w_*\left[\left(\frac{u_*}{w_*}\right)^3\left(1.6 - \frac{z}{z_i}\right)^{3/2} + 1.2\frac{z}{z_i}\left(1 - 0.98\frac{z}{z_i}\right)^{3/2}\right]^{1/3} \tag{4}$$

$$\overline{w^3}(z) = 0.84w_*^3\frac{z}{z_i}\left(1 - \frac{z}{z_i}\right) \tag{5}$$

$$S_w(z) = \frac{\overline{w^3}}{\sigma_w^3}, \tag{6}$$

where z_i is the depth of the CBL, σ_w the standard deviation of w, S_w the skewness of w, w_* the convective velocity scale, and u_* the surface friction velocity. Still following Weil (1990), the upward and downward mean velocities at any height in the

convective updrafts and downdrafts can be estimated using

$$w_u(z) = \sigma_w(z)[0.21 S_w(z) + 0.5(0.18 S_w^2(z) + 1.23)^{1/2}] \quad (7a)$$

$$w_d(z) = \sigma_w(z)[0.21 S_w(z) - 0.5(0.18 S_w^2(z) + 1.23)^{1/2}]. \quad (7b)$$

We define D_u and D_d as the horizontal, geometric dimensions of the updrafts and downdrafts (i.e., their diameters), respectively, such that D $(=D_u + D_d)$ is the total "wavelength" of each pair. We also define the ratio R as

$$R = \frac{-\overline{w_d}}{\overline{w_u}} = \frac{D_u}{D_d}, \quad (8)$$

where the overbar represents the vertical average of the vertical velocities in (7) from the surface to z_i and the value of R depends on the skewness of the vertical velocity components. For typical conditions of the afternoon of day 33 of the Wangara experiment, R is about 0.5. We require that at any altitude, the integrated upward mass flux in the updraft area be equal to the downward mass flux in the downdraft for mass conservation, which can be expressed as

$$D_u w_u(z) = -D_d w_d(z). \quad (9a)$$

However, Weil's w_u and w_d in (7a) and (7b) do not exactly satisfy this constraint. Hence, we use $w_u(z)$ calculated with (7a) and R to compute $w_d(z)$:

$$w_d(z) = -R w_u(z). \quad (9b)$$

The downward velocities so calculated are then consistent with mass conservation. We choose to use (7a) and $w_u(z)$ rather than (7b) and $w_d(z)$ because (7b) does not approach zero monotonically at $z \approx z_i$ as (7a) does.

In this model we assume w varies sinusoidally in the horizontal, with amplitudes proportional to those computed with (7a). We also assume that the *dimensions* of each updraft and downdraft are constant with height and invariable in the horizontal. This is not exactly true in nature, but appears as for most of the vertical extent of the CBL (Stull 1988) and should not have a significant impact on the model's predictions. With these assumptions, the initial horizontal distribution of vertical velocities over one "wavelength" at any height is given for updrafts by

$$w(x, z) = C_w w_u(z) \sin\left(\frac{\pi}{D_u} x\right) \quad \text{if} \quad 0 \leq x \leq D_u \quad (10a)$$

and for downdrafts by

$$w(x, z) = -R C_w w_u(z) \sin\left[\frac{\pi}{D_d}(x - D_u)\right] \quad \text{if} \quad D_u < x \leq D. \quad (10b)$$

The parameter of C_w is needed to scale $w_u(z)$ since (7a) gives the average updraft speed (Weil 1990). The average of the sine over half a wavelength is 0.64 times its amplitude, so we expected $C_w \approx 1/0.64 = 1.6$ (In fact, $C_w \approx 2.6$ is needed to reproduce the experimental results.) During the time integration, this sinusoidal pattern is renewed (generated) at the upstream boundary and advected through the domain such that

$$\frac{\partial w(z, t)}{\partial t} = -U_a \frac{\partial w}{\partial x}, \quad (11)$$

where U_a is the vertically averaged horizontal mean wind speed in the CBL. The horizontal periodic component u is computed from the vertical w distribution using the continuity equation (3). At the upstream boundary, the analytic integrals of (10) are used to determine u:

$$u(x, z) = \begin{cases} C_w \dfrac{D_u}{\pi} \dfrac{\partial w_u}{\partial z} \cos\left(\dfrac{\pi}{D_u} x\right), & 0 \leq x \leq D_u \quad (12a) \\ -C_w R \dfrac{D_d}{\pi} \dfrac{\partial w_u}{\partial z} \cos\left[\dfrac{\pi}{D_d}(x - D_u)\right], & D_u < x \leq D. \quad (12b) \end{cases}$$

An instantaneous view of the horizontal variation of w at $z = 0.5 z_i$ is shown in Fig. 1a for $C_w = 2.6$, $R = 0.5$, and $D = 1200$ m. Figure 1b shows the perturbation velocity vector in an x–z plane for one pair of up and down drafts.

The horizontal scale D needs to be specified. Hunt et al. (1988) report the wavelength of the peak in the spectra of w is the order of z_i. Stull (1988) suggests that the combined linear dimension of updraft and downdraft pairs is also the order of z_i. We therefore define D as

$$D = C_d z_i,$$

where we expect C_d to be near unity.

The eddy diffusivity K_h in the model is estimated using a local Richardson number–dependent scheme proposed by Blackadar (1979):

$$K_h = l^2 S(1 - 87\mathrm{Ri})^{1/2}, \quad \mathrm{Ri} < 0$$

$$K_h = l^2 S\left(1 - \frac{\mathrm{Ri}}{\mathrm{Ri}_c}\right)^2, \quad \mathrm{Ri} \geq 0, \quad (13)$$

where local Richardson number Ri and mixing length l are calculated as

$$\mathrm{Ri} = \frac{g}{\theta_v S^2} \frac{\partial \theta_v}{\partial z},$$

$$l = \frac{\kappa z}{1 + (\kappa z/\lambda)},$$

and S is the vertical shear of the horizontal wind, θ_v the virtual potential temperature, l the mixing length,

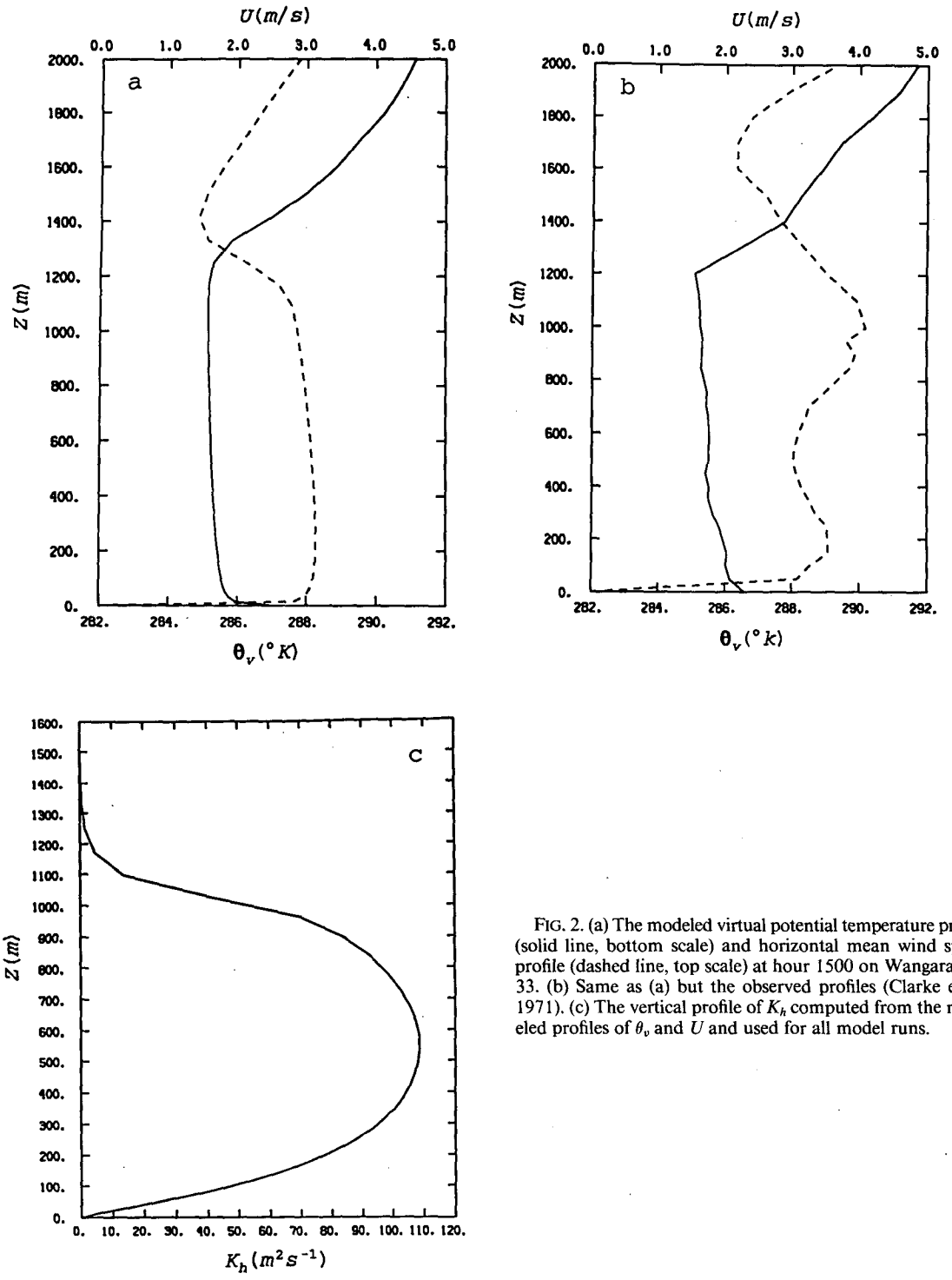

FIG. 2. (a) The modeled virtual potential temperature profile (solid line, bottom scale) and horizontal mean wind speed profile (dashed line, top scale) at hour 1500 on Wangara day 33. (b) Same as (a) but the observed profiles (Clarke et al. 1971). (c) The vertical profile of K_h computed from the modeled profiles of θ_v and U and used for all model runs.

and λ a scale proportional to the PBL depth. The critical Richardson number Ri_c is set to be 0.25.

At first one might expect that K_h would be considerably smaller than that given by (13), since in this model the explicit vertical advections would preclude the large eddy diffusivities needed to accomplish strong vertical diffusion in the absence of explicit advections. However, only a slight reduction in the value of K_h in most of the modeled CBL could be made and still obtain good agreement with the WD experimental results. It appears that the role of the coherent advections is primarily to displace the plume concentration centerline, while the diffusion across the centerline is dominated by the subgrid-scale eddies, and, hence, K_h must

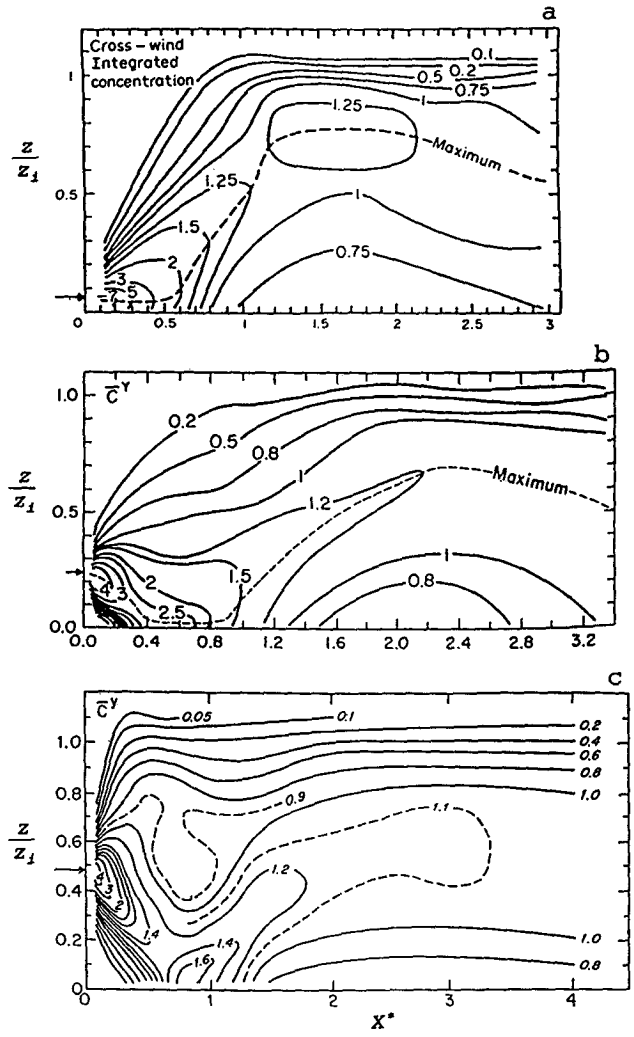

FIG. 3. Nondimensional crosswind-integrated concentration C_y^* fields measured in the laboratory experiments for sources of height $Z_s = 0.067z_i$ (a), $0.24z_i$ (b), and $0.49z_i$ (c) (Willis and Deardorff 1976, 1978, 1981).

remain large. The best model–experiment agreement was obtained with $\lambda = 0.067z_i = 80$ m, which is the value used throughout the results reported here.

3. Numerical techniques

The domain width X is 10 000 m and the depth is 2000 m. The horizontal grid points are equally spaced with $\Delta x = 50$ m. The vertical grid space is expanded in a logarithmic coordinate with the 1st layer being 15 m thick and the 40th and top-most layer being 100 m thick. The diffusion effects in (1) are evaluated on this expanding grid using a semi-implicit technique described in Carroll (1993). Vertical and horizontal advections are computed using a Crowly type of Warming–Kutler–Lomax scheme (Anderson et al. 1984; Huang and Raman 1991) in time-split method. The scheme is set to be fully third-order accurate. A mass-conserving filter (Seibert and Morariu 1991) is used to suppress numerical modes. The time step is 10 s, yielding a horizontal Courant number $U_a\Delta t/\Delta x \leq 0.7$, a vertical Courant number of less than or equal to 0.3, and a diffusive stability parameter $(K/\Delta z^2)_{\max}\Delta t \leq 1.2$, which is numerically stable for the semi-implicit diffusion calculations.

The model calculations are all performed with the conditions on Wangara day 33 at hour 1500 (Clarke et al. 1971). The mean wind, eddy diffusivity, and potential temperature profiles are obtained from the output of a PBL model (Carroll 1993) applied to simulate Wangara day 33. The profiles of modeled and observed temperature and mean wind are shown in Figs. 2a,b, while the vertical profile of calculated K_h using $\lambda = 80$ m within the fully developed mixed layer is shown in Fig. 2c. At this time, the CBL depth, defined as the height where the vertical gradient of potential temperature first becomes positive, is 1170 m. At the same time, $w_* = 1.36$ m s^{-1}, $u_* = 0.17$ m s^{-1}, and the Obukhov length $L = -7$ m.

A source of an inert tracer is placed 10 m upwind of the left-hand boundary. To avoid problems with the advection scheme's boundary conditions and to allow the emitted plume to grow to grid-resolvable scale, we follow the common modeling practice of allowing the plume to travel three grid points into the domain while dispersing in the manner described by the standard Gaussian dispersion model for a continuous line source, that is,

$$C_y(x, z) = \frac{Q}{(2\pi)^{1/2}\sigma_z(x)U(Z_s)}\left\{\exp\left[-\frac{(Z_s - z)^2}{2\sigma_z^2(x)}\right] + \exp\left[-\frac{(Z_s + z)^2}{2\sigma_z^2(x)}\right]\right\}. \quad (14)$$

Here $\sigma_z = [2K_h(x + 10)/U]^{0.5}$ is the standard deviation of the Gaussian distribution of the concentration about the plume centerline in the vertical at downwind distance x, Z_s is the effective source height, U is the wind speed at Z_s, z is the height above the ground, and Q (kg m^{-1} s^{-1}) is the line source strength. An open boundary condition is applied at the right lateral boundary.

Equation (1) predicts the quasi-instantaneous concentrations at a point. The variable of interest is the time-averaged concentration. The concentrations at each point are averaged over time starting when the initially emitted material has traveled through the domain, about 50 min into the simulation. Given the nature of the model, averaging over one period ($D/U_a = 400$ s) is sufficient to reproduce all the major features of the WD results, but the output fields are somewhat noisy. We believe this is due to aliasing or truncation errors; that is, the concentrations calculated at the grid points for only one plume cycle cannot provide smooth contours. Results presented here were averaged over 12 cycles and are expressed in terms of the dimensionless crosswind-integrated concentration C_y^* and the dimensionless downwind distance X^*:

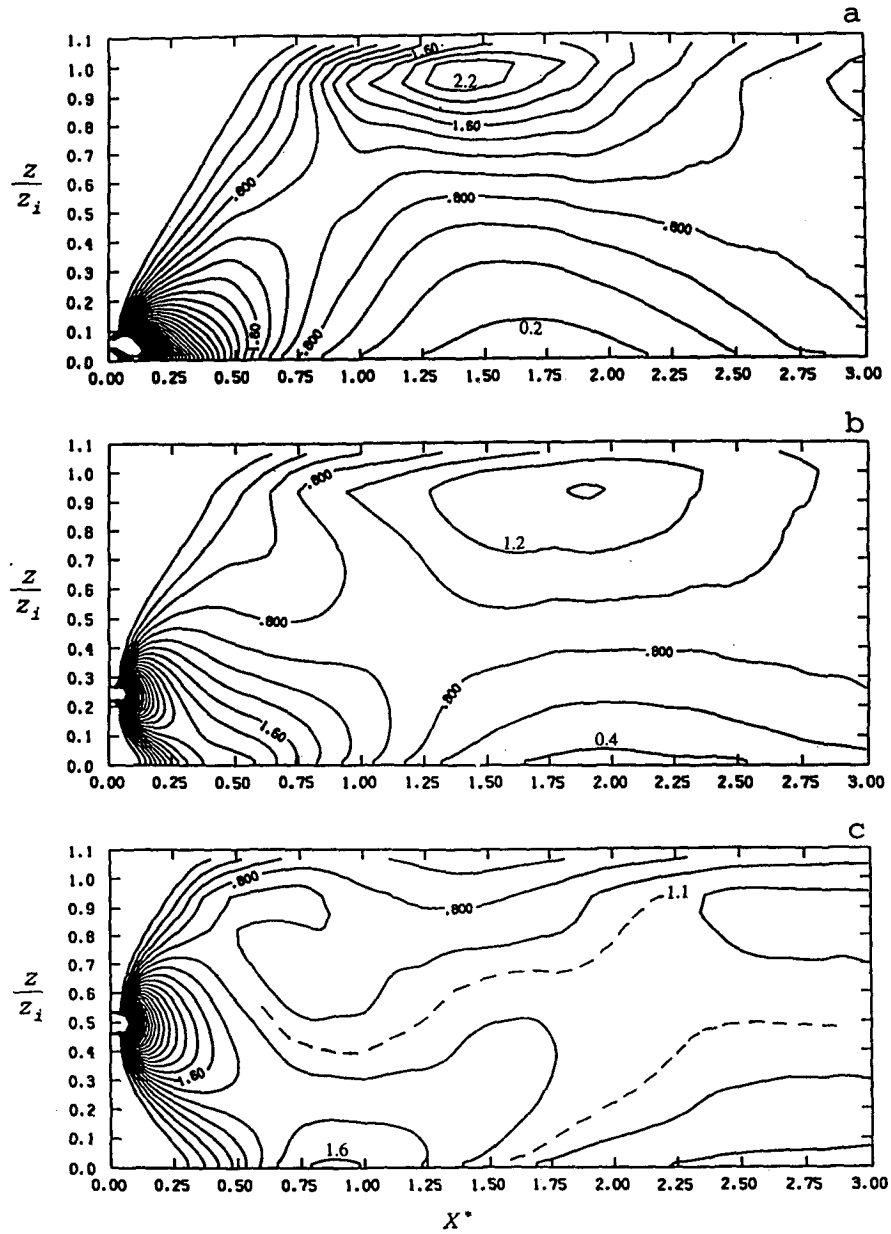

FIG. 4. Nondimensional crosswind-integrated concentration C_y^* fields simulated by the present model for sources of height $Z_s = 0.058z_i$ (a), $0.24z_i$ (b), and $0.50z_i$ (c). Contour interval is 0.2.

$$C_y^* = \frac{U_a z_i C_y}{Q}$$

$$X^* = \frac{w_* X}{U_a z_i}. \qquad (15)$$

Using (14) to initially disperse the emitted material introduces some uncertainty as to where the source is located in the model (i.e., where is $X^* = 0$?). In fact, the difference between placing the source at $x = -10$ or at $x = 150$ m gives a variation in ΔX^* being less than 0.06.

4. Model dispersion experiments

All results discussed in this section were obtained with $R = 0.5$, $C_w = 2.6$, $D = 1200$ m, and $C_d = 1.03$. The choice of $D = 1200$ m is simply more convenient than $D = z_i = 1170$ m. The R value is determined by the vertical velocities computed with (7), averaged in the vertical, and rounded to the nearest tenth for convenience. The value of C_w was found by numerical experiments, which were necessary to reproduce as closely as possible WD laboratory results (cf. Fig. 3). Sensitivity of model predictions to these choices is examined in the next section. Here we present the best

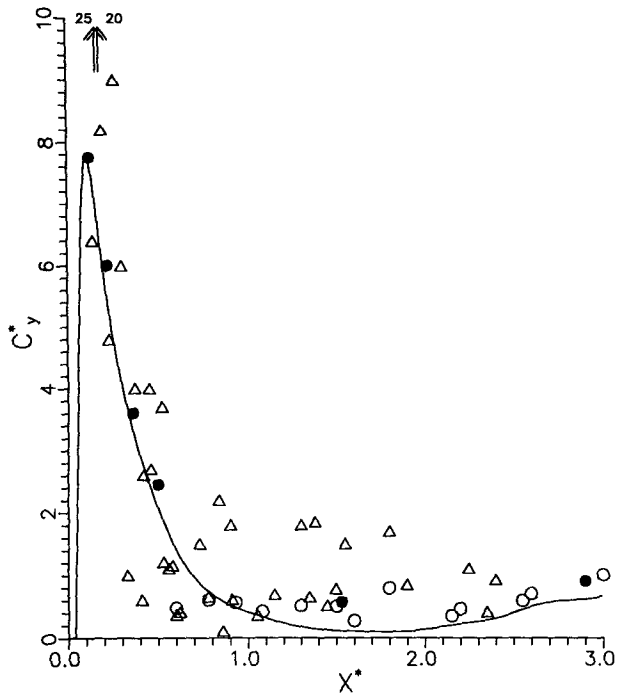

FIG. 5. Plot of ground-level concentrations C_y^* versus downwind distance X^* for near-ground releases. Solid line is from the present model; solid circles the WD laboratory; open circles the CONDORS chaff experiment; triangles the CONDORS oil, in which two large concentrations of 25 and 20 are arrow marked.

results obtained using sinusoidal wave forms, an example of CBL conditions (i.e., the Wangara experiment), and the chosen definitions of R and D.

Three cases are presented, corresponding to dispersion from continuous sources at heights $Z_s = 0.058z_i$, $0.24z_i$, and $0.50z_i$. The distribution of the time-averaged, crosswind-integrated dimensionless concentrations for the three release heights are shown in Fig. 4.

TABLE 1. Sensitivity to vertical velocity scaling C_w ($R = 0.5$, $D = 1200$ m).

C_w	1.00	1.50	2.00	2.50	3.00	3.50	4.00
$M/425$	0.38	0.58	0.77	0.96	1.15	1.35	1.54
$C_{sfc}/1.63$	0.79	0.87	0.92	0.98	1.03	1.07	1.12
$X_{sfc}/0.87$	2.02	1.48	1.29	1.02	0.89	0.81	0.74
$C_{elv}/2.34$	0.57	0.73	0.90	1.00	1.03	1.03	1.05
$X_{elv}/1.39$	2.15	1.76	1.36	1.03	0.96	0.72	0.69

a. Case 1 (Fig. 4a)

A near-ground release at $Z_s = 0.058z_i$ ($Z_s = 68$ m). The maximum concentration centerline (e.g., the locus of maximum concentrations) first moves parallel to the surface and then starts to rise rapidly at the downwind distance $X^* = 0.5$, being carried aloft by updrafts. The dispersion pattern in the lower part of the mixed layer matches very well that of the laboratory experiments (cf. Fig. 3a). The elevated concentration maximum reaches a height of $z = 0.93z_i$ at about $X^* = 1.40$. This is the same distance downwind as observed in the laboratory experiments, but the height is higher ($z = 0.75z_i$ in WD), and the concentrations are greater than observed in the laboratory. These differences are also seen in the results from most other models (Lamb 1982; Enger 1986; Sawford and Guest 1987; Luhar and Britter 1989). At about $X^* = 2.0$, the centerline begins to descend back into the middle of the CBL in a manner similar to the laboratory results.

The greater elevation and higher-modeled concentrations near the upper boundary in this case may be

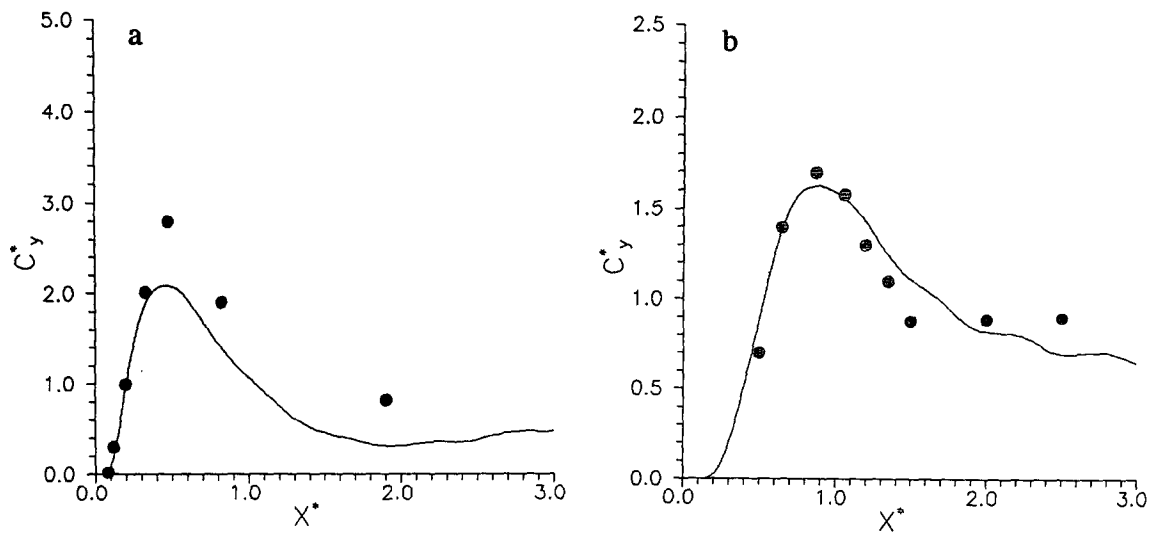

FIG. 6. The modeled ground-level concentrations C_y^* (solid lines) compared with the corresponding values from the WD laboratory experiments (solid circles). Source height at $0.24z_i$ (a) and $0.50z_i$ (b).

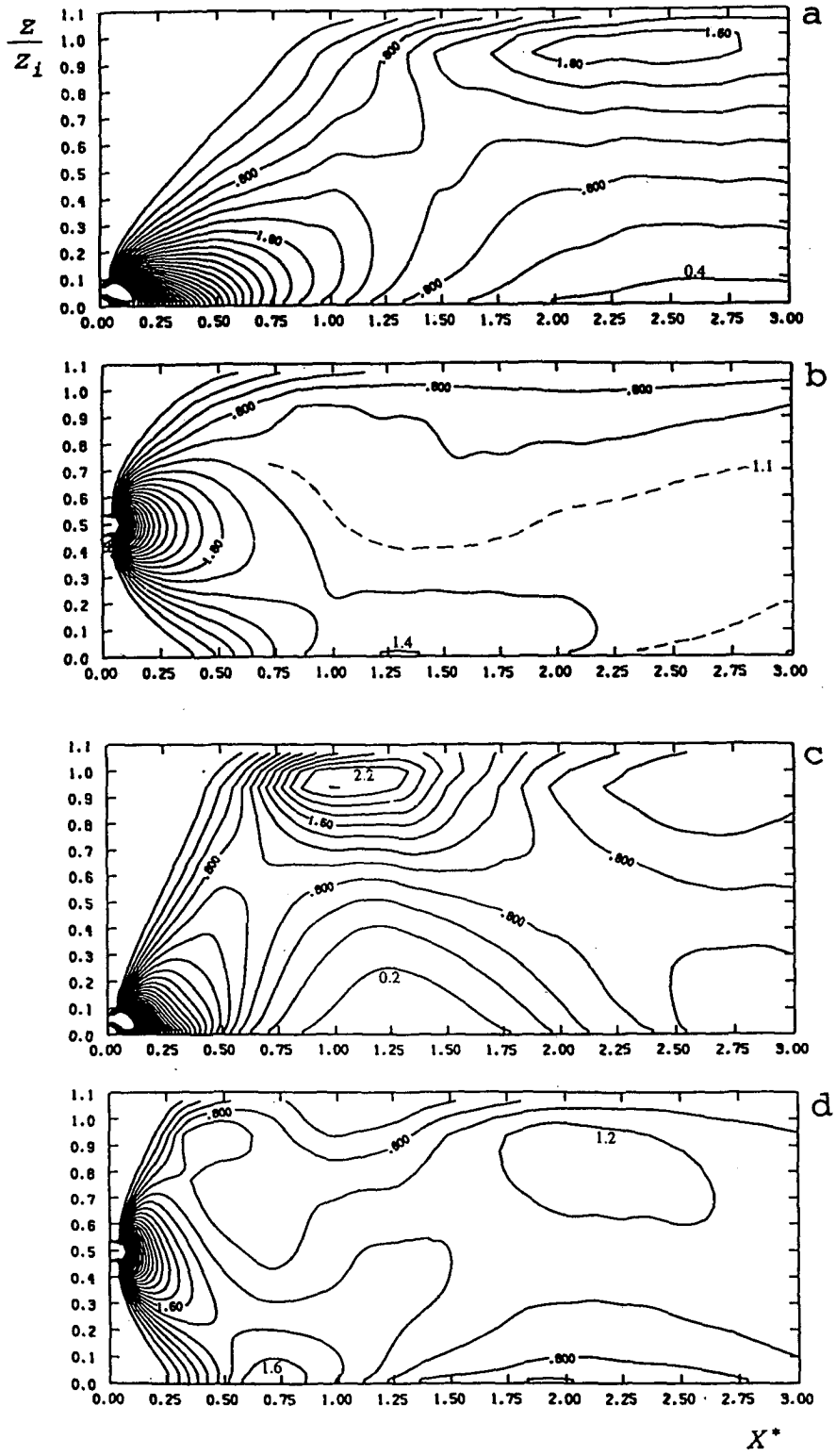

FIG. 7. Nondimensional crosswind-integrated concentration C_y^* fields using $C_w = 1.5$ [(a), (b)] compared with those using $C_w = 3.5$ [(c), (d)] but the standard $R = 0.5$ and $D = 1200$ m for source heights $Z_s = 0.058z_i$ [(a), (c)] and $0.50z_i$ [(b), (d)]. Contour interval is 0.2.

TABLE 2. Variations with down-to-updraft ratio R (C_w = 2.6, D = 1200 m).

R	0.26	0.33	0.41	0.50	0.60	0.71	0.85
M/425	0.62	0.75	0.87	1.00	1.13	1.25	1.38
C_{sfc}/1.63	0.88	0.91	0.95	1.00	1.03	1.06	1.07
X_{sfc}/0.87	1.48	1.36	1.15	1.00	0.89	0.81	0.71
C_{elv}/2.34	0.76	0.85	0.96	1.00	1.04	1.03	1.03
X_{elv}/1.39	1.36	1.12	1.06	1.00	0.97	0.96	0.91

due to insufficient diffusion near the CBL top, due to a lack of kinematic similarity between the modeled atmospheric behavior near z_i and the water tank experiments, or due to the sparsity of observations of σ_w and S_w in the upper CBL, reducing the confidence in parameterizations (4) and (5) for $z > 0.5z_i$. We note that while most numerical models and the WD experiments show an elevated maximum between $X^* = 1$ and 2.5 the CONDORS (convective diffusion observed with remote sensors) results do not. Manipulating the K_h scaling improves the results aloft to some degree, but at the price of significant loss of agreement in the rest of the CBL.

The ground-level concentrations from this model of case 1, averaged over the lowest two model layers ($0 < z \leq 0.027z_i$), from the WD laboratory data collected at $z \approx 0.025z_i$, and from the CONDORS field experiments (Briggs 1993, Fig. 19) are plotted in Fig. 5 for near-ground releases. Noting that near the source ($X^* < 0.2$), the vertical and horizontal gradients in concentrations are very large so that small variations in the source height, receptor height, or downwind sampling position can result in large differences in observed concentrations. The near-source CONDORS data (i.e., $6.4 \leq C_y^* \leq 25$ for $X^* \leq 1.0$), our model, and the tank experiments show excellent agreement and all lie within the range of observed concentrations. For $1.0 \leq X^* \leq 2.5$, the modeled minima are systematically less than the field and laboratory measurements. At $X^* \geq 2.5$, the observed and modeled concentrations approach 1, that is, the well-mixed values.

b. Case 2 (Fig. 4b)

A low-altitude source at $Z_s = 0.24z_i$ (Z_s = 284 m). In this case, the concentration centerline first falls due to large areas of downdrafts, reaching the ground at $X^* = 0.46$ and creating a local maximum ($C_y^* = 2.2$) there. The plume stays near the ground for a short distance, then starts to lift off at $X^* = 0.80$. The modeled centerline ascends to $z = 0.9z_i$ with an elevated local maximum concentration $C_y^* = 1.4$ at about $X^* = 1.9$. Eventually the centerline descends slowly, and concentrations become well mixed farther downwind. All these characteristics compare well with the laboratory experiments (see Fig. 3b). The ground-level maximum occurs at the same X^*, with a concentration about 14% lower than the laboratory result. The CONDORS results (Briggs 1993, Fig. 20, chapter 34) shows a higher ground-level maximum ($C_y^* = 3$) at greater distance, $X^* = 0.8$. The downwind minimum (within $1.7 \leq X^* \leq 2.5$) is smallest in our model, being about half that of the WD experiments. In the CONDORS data, this minimum is farther downwind, with larger concentrations than in our model or the laboratory experiments. The greatest disparity between the model and the laboratory experiments again occurs in the upper part of the mixed layer near the source.

Figure 6a shows the modeled ground-level concentrations for this $Z_s = 0.24z_i$ case and the corresponding WD experimental data. The calculated values are consistently about one-third lower than those obtained in the laboratory. This discrepancy is common to most other model simulations (e.g., Baerentsen and Berkowicz 1984; de Baas et al. 1986; Sawford and Guest 1987).

c. Case 3 (Fig. 4c)

A midlevel elevated source at $Z_s = 0.50z_i$ (Z_s = 580 m). The numerical simulation is in very good agreement with the laboratory experiments (Fig. 3c). The plume centerline descends rapidly, impinging on the ground at $X^* = 0.87$, with a maximum concentration there of $C_y^* = 1.63$. Both these features match very well with the WD experiments. The distance to the surface maximum also matches the CONDORS well, but both our concentrations and the WD's are about 40% lower than the field data. The plume then rebounds strongly from the surface, producing a second line of high concentrations that rises to $z = 0.85z_i$. This strong "liftoff" is caused by strong horizontal convergence near the ground in the coherent structures. If we turn off the convergence calculations (i.e., $u \equiv 0$), we do not see the plume rebound from the ground for any of the elevated sources. Again, major differences between the model and the laboratory experiments occur near the top of the mixed layer at small X^*. The Chatfield and Brost (1987) model does not explicitly evaluate the local convergence and does not show plume liftoff, characteristic of the CBL. The calculated ground-level concentrations in this case are in close agreement with the laboratory results (cf. Fig. 6b).

We note that our results are generally much closer to the experimental results than those of most other models, including Lagrangian models with skewed vertical velocities. We believe this is true because in our model a realistic temporal and spatial coherence between w and u is maintained, whereas in a random walk model or stochastic model u and w are independent of each other; that is, they are not coupled through the continuity equation. Our experience, that poor results are found if u is not calculated, illustrates the importance of horizontal divergence and convergence effects near the ground and at the top of the mixed layer to dispersion in convective conditions.

In terms of computational efficiency, this model is much faster than, for example, Weil's (1990) Lagran-

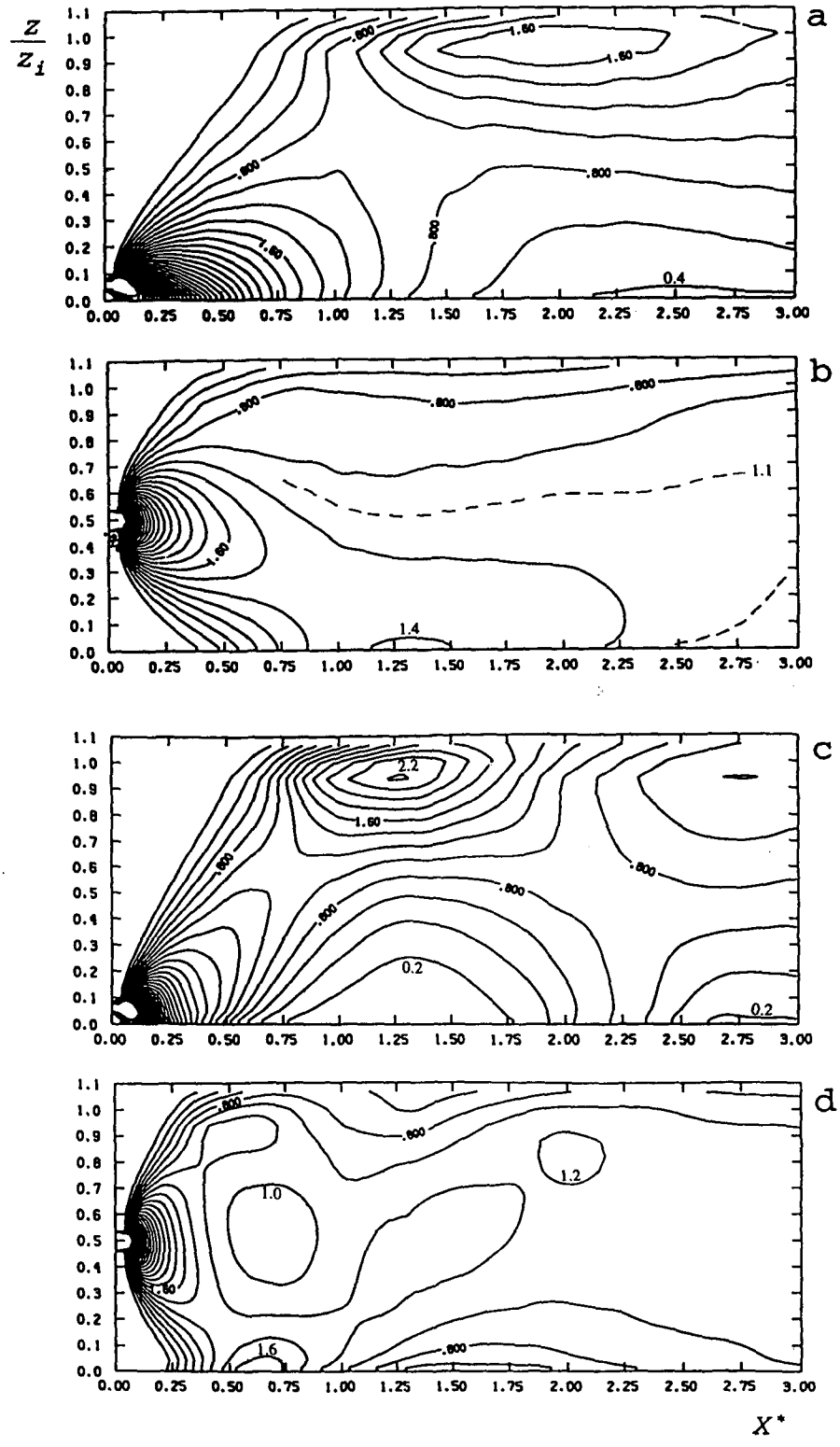

FIG. 8. Same as Fig. 7 but for $R = 0.26$ [(a), (b)] and 0.85 [(c), (d)] and the standard $C_w = 2.6$ and $D = 1200$ m.

TABLE 3. Variation with R and C_w (D = 1200 m, M = 425 m^2 s^{-1}).

R	0.26	0.33	0.41	0.50	0.60	0.71	0.85
C_w	4.20	3.48	2.98	2.60	2.30	2.07	1.88
$C_{sfc}/1.63$	0.98	0.98	0.99	1.00	1.01	1.00	0.99
$X_{sfc}/0.87$	1.12	1.09	1.02	1.00	0.98	0.93	0.91
$C_{elv}/2.34$	0.96	1.00	0.99	1.00	1.00	0.98	0.97
$X_{elv}/1.39$	0.94	0.96	0.97	1.00	1.04	1.07	1.12

gian model. We have experimented with the latter (Scott 1994) in a domain 1000 m deep and 16 km long with Δx = 200 m and Δz = 50 m (i.e., 1600 grid points). For statistical stationarity and relatively smooth concentration fields, 20 000 particles need to be released. On a VAX station 4000, the 20 000-particle Weil model required about 30 times the computation time as the current model in a similarly sized domain but with 8000 grid points.

5. Sensitivity tests

There are two free parameters in the model (C_w and C_d) whose effects on model prediction should be explored. In addition, the ratio R is a key parameter but not a free one in the sense that it varies inversely as the skewness of w (i.e., as $|S_w| \to 0$, $R \to 1$ and as $S_w \to +\infty$, $R \to 0$). We chose to vary R rather than S_w explicitly since the physical meaning of R in the model is more apparent.

Since (7) gives mean vertical velocities, C_w is needed to scale the amplitudes of the sine functions in (10) and was expected to be about 1.6. The need for C_w to be greater than 2 to achieve results comparable to the WD experiments is not well understood at this writing. There are several "unrealistic" assumptions made in the model design: (a) that w varies sinusoidally in the horizontal; (b) that updraft and downdraft dimensions are constant with height; and (c) that the convective plumes move downwind at a mean, vertically invariant speed. In several numerical experiments we changed the horizontal form of the w variation to approach a square wave by using fractional powers of the sine functions in (10). Even using $\sin^{0.25}$, $C_w \approx 2$ is required to obtain results similar to those in Fig. 4. Hence, we chose to stay with the basic sine function to describe the convective plumes and can only comment that C_w appears to be the parameter that compensates for a number of unrealistic model attributes. It is also quite possible that Weil's formulas (7a,b) underestimate the vertical velocity magnitudes.

For the purposes of the sensitivity analysis, we used cases 1 and 3 with R = 0.5, C_w = 2.6, and C_d = 1.03 as the control runs. For the near-ground release (case 1), we chose the evaluation criteria to be the nondimensional elevated maximum concentration C_{elv} and the nondimensional downwind distance X_{elv} at which it occurs. The height at which C_{elv} occurs is nearly constant for all runs. For the mid-CBL release (case 3), we chose for comparison the maximum surface concentration C_{sfc} and the downwind distance X_{sfc} at which this maximum occurs. We also computed the total kinematic vertical transport rate across the middle of the CBL in one updraft or one downdraft as

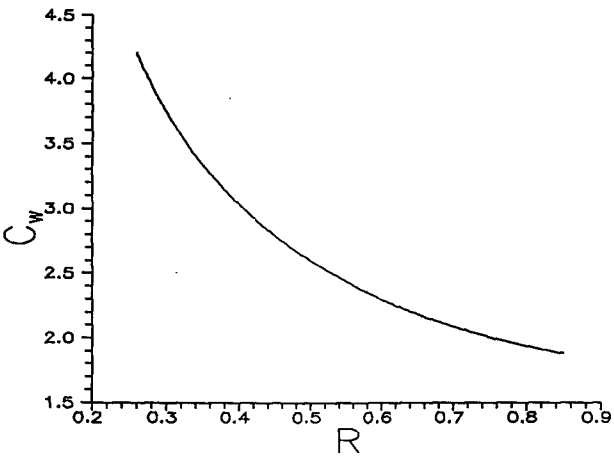

FIG. 9. Plot of C_w versus R for constant M ($\approx$425 m^2 s^{-1}) and D = 1200 m.

$$M = \int_0^{D_u} w(x, 0.5z_i)dx = -\int_{D_u}^{D} w(x, 0.5z_i)dx, \quad (16a)$$

or, using the average of the sine function in (10)

$$M = 0.64C_w w_u D_u = 0.64RC_w w_u(D - D_d R), \quad (16b)$$

where w_u is at the middle of z_i. We include the second definition in (16b) to show the relationship of M to D_d. The results are expressed as the ratios of the test run values to their values from the control runs.

Sensitivity to C_w was examined holding R and C_d fixed. Increasing C_w increases the magnitude of the vertical speeds and hence the rate of advection in the convective plumes (i.e., M increases). As shown in Table 1, the maximum concentrations for both elevated and ground-level sources increase with increasing C_w, whereas the downwind distances to the maxima decrease; that is, stronger vertical motions force low-level releases to loft sooner and elevated sources to reach the ground sooner. The concentration patterns for C_w = 1.5 and C_w = 3.5 are shown in Fig. 7 for the elevated

TABLE 4. Variation with total size $D = C_d z_i$ (R = 0.5, C_w = 2.6).

C_d	0.51	0.77	1.03	1.28	1.54	1.80	2.05
$M/425$	0.49	0.75	1.00	1.25	1.51	1.76	2.01
$C_{sfc}/1.63$	0.97	1.02	1.00	0.99	0.96	0.93	0.90
$X_{sfc}/0.87$	1.07	1.05	1.00	1.00	1.05	1.05	0.98
$C_{elv}/2.34$	0.88	1.02	1.00	0.94	0.94	0.97	0.89
$X_{elv}/1.39$	1.09	1.09	1.00	0.91	0.94	1.01	1.01

and ground-level sources. We can see that a strong rebound of the plume centerline from the vertical boundaries of the CBL occurs with large C_w. For $C_w < 1.0$ (not shown), the vertical displacement of the centerline is so slow that, in the domain used, the concentration distribution is very similar to that calculated with a traditional Gaussian or pure K-theory model.

Sensitivity to R, which represents the skewness, was examined holding C_w and D fixed and varying R such that D_u, D_d, and $w_d(z)$ change accordingly. The results are shown in Table 2. In this test, $w_u(z)$ and w_d are obtained using (7a) and (9b), respectively, so that the mass conservation expressed in (9a) is maintained. With increasing R, S_w decreases and the concentration distribution for the midlevel source becomes more symmetric about the height of release as shown in Fig. 8. For both elevated and ground-level sources, the maximum concentrations increase with increasing R, while the downwind distance for the plume to hit the ground or reach the upper mixed layer decreases. This seems counterintuitive in that, as the skewness decreases, we would expect that plume lifting in case 1 and that plume sinking in case 3 would occur later rather than sooner. However, $w_u(z)$ is still computed from (7a) for the same stability conditions. As $R \rightarrow 1$ (i.e., $S_w \rightarrow 0$), its duration relative to $w_d(z)$ increases as does upward mass flux, so lofting of the low-level source plume can occur more rapidly. For the midlevel source, as $R \rightarrow 1$, the magnitudes of w_d and w_u become more equal (i.e., w_d increases), so the vertical transport becomes more symmetrical about middle level and the net rate of transport to each boundary is a little faster.

Given the above results, we changed R and C_w together such that M is held essentially constant ($\approx$425 $m^2\ s^{-1}$) with fixed D. The results are shown in Table 3. Clearly, choosing combinations of R and C_w such that M is constant gives essentially the same maximum concentrations at about the same distances downwind from the sources. The value of M is about 425 $m^2\ s^{-1}$ for the Wangara conditions. The combinations of C_w and R that produce this value of M are plotted in Fig. 9.

We expected that sensitivity of the model results to changes in C_d would be very weak, provided the ratio $\Delta x/D$ is sufficiently small ($\leq$0.05) that the modeled convective plumes are well resolved within the grid. As can be seen from (16), M, and therefore the quality of the results, depends somewhat on D and therefore C_d. The sensitivity to C_d for fixed R and C_w are shown in Table 4. For $0.75 < C_d < 1.50$, the model results are not significantly different. Clearly, much larger variations in C_d would not be physically realistic; that is, the horizontal dimension of the plume pairs is not likely to be much greater or much smaller than the CBL depth.

6. Summary and conclusions

The model is relatively simple but, with reasonable choices of parameter values, appears to reproduce the experimental results as well as those obtained from far more complex models. The concept on which it is based is physically realistic and reflects the commonly accepted view of the effects of coherent structures on CBL dispersion. Except at the CBL top, near the source, the model and experimental concentration distributions are qualitatively the same. The model parameters such as R and C_d are clearly constrained by physical conditions and observations. The need for C_w to be 2.6 instead of the expected value of 1.6 has not been fully explained but is probably due to possible underestimates by Weil's original formulas and the unrealistic geometric constraints we imposed on the model convective plumes. The calculated ground-level concentrations are well reproduced for midlevel release but are only about two-thirds of observed values for $Z_s \approx 0.25 z_i$. For near-ground releases, the model reproduces the maximum ground-level concentration well for $X^* \leq 1$ but underestimates the minimum around $X^* \approx 2$.

We used conditions for the afternoon of day 33 of the Wangara experiment to predict these concentrations. This choice simply provides realistic convective conditions, while the general agreement between the scaled model and experimental results indicates the generality of these conclusions. The finding that the vertical flux parameter M must acquire a particular value to produce a realistic result is logical, given that skewed vertical fluxes are the cause of asymmetric vertical dispersion. The value of R is not arbitrary but determined by the skewness of the vertical velocity distribution. It is not clear at this writing that $M \approx 425$ $m^2\ s^{-1}$ is a general criterion, but we suspect it is. If so, given R, C_w can be estimated from Fig. 9. With $C_d \approx 1$, the model parameters are fully defined.

Our numerical experiments indicate that K_h needs to be nearly as large as the original Blackadar parameterization used in CBL modeling. This suggests that incoherent turbulent eddy mixing is still an important process, diffusing material about the axes of maximum pollutant concentration. The role of the coherent convective plumes is to control the vertical migrations of these axes.

Acknowledgments. This work was supported in part by the Ecotoxicology Program of the University of California Toxic Substances Research and Training Program. This work was also supported in part by the U.S. EPA (R814709) Center for Ecologic Health Research at UC Davis. The information presented may not necessarily reflect the views of the EPA, and no official endorsement should be inferred. The support of the University of California Division of Agriculture and Natural Resources is also acknowledged.

REFERENCES

Anderson, D. A., J. C. Tannehill, and R. H. Pletcher, 1984: *Computational Fluid Mechanics and Heat Transfer.* McGraw-Hill, 599 pp.

Andre, J. C., G. D. Moor, P. Lacarrere, G. Therry, and R. D. Vachat, 1978: Modeling the 24-hour evolution of the mean and turbulent structures of the planetary boundary layer. *J. Atmos. Sci.*, **35,** 1861–1882.

Baerentsen, J. H., and R. Berkowicz, 1984: Monte Carlo simulation of plume dispersion in the convective boundary layer. *Atmos. Environ.*, **18,** 701–712.

Blackadar, A., 1979: High-resolution models of the planetary boundary layer. *Advances in Environmental Sciences and Engineering,* Vol. 1, J. R. Pfafflin and E: N. Ziegler, Eds., Gordan and Breach Publ., 50–82.

Briggs, G. A., 1993: Plume dispersion in the convective boundary layer. Part II: Analyses of CONDORS field experiment data. *J. Appl. Meteor.*, **32,** 1388–1425.

Carroll, J. J., 1993: Sensitivity of PBL model prediction to model design and uncertainties in environmental inputs. *Bound.-Layer Meteor.*, **65,** 137–158.

Chatfield, R. B., and R. A. Brost, 1987: A two-stream model of the vertical transport of trace species in the convective boundary layer. *J. Geophys. Res.*, **92,** 13 263–13 276.

Clarke, R. H., A. J. Dyer, R. R. Brook, D. G. Ried, and A. J. Troup, 1971: The Wangara experiment: Boundary layer data. Div. Met. Phys. Tech. Paper 19, CSIRO, 225–240.

Deardorff, J. W., 1974: Three-dimensional study of the height and mean structure of a heated planetary boundary layer. *Bound.-Layer Meteor.*, **7,** 81–106.

de Bass, A. F., H. van Dop, and F. T. M. Nieuwstadt, 1986: An application of the Langevin equation for inhomogeneous conditions to dispersion in a convective boundary layer. *Quart. J. Roy. Meteor. Soc.*, **112,** 165–180.

Enger, L., 1986: A higher order closure model applied to dispersion in a convective PBL. *Atmos. Environ.*, **20,** 879–894.

Gao, W., R. H. Shaw, and K. T. Paw U, 1989: Observation of organized structure in turbulent flow within and above a forest canopy. *Bound.-Layer Meteor.*, **47,** 349–377.

Huang, C., and S. Raman, 1991: A comparative study of numerical advection schemes featuring a one-step modified WKL algorithm. *Mon. Wea. Rev.*, **119,** 2900–2918.

Hunt, J. C. R., J. C. Kaimal, and J. E. Gaynor, 1988: Eddy structure in the convective boundary layer—New measurements and new concepts. *Quart. J. Roy. Meteor. Soc.*, **114,** 827–858.

Hurley, P., and W. Physick, 1993: A skewed homogeneous Lagrangian particle model for convective conditions. *Atmos. Environ.*, **27A,** 619–624.

Huynh, B. P., C. E. Coulman, and T. R. Turner, 1990: Some turbulence characteristics of convectively mixed layers over rugged and homogeneous terrain. *Bound.-Layer Meteor.*, **51,** 229–254.

Kaimal, J. C., J. C. Wyngaard, D. A. Haugen, O. R. Cote, and Y. Izumi, 1976: Turbulence structure in the convective boundary layer. *J. Atmos. Sci.*, **33,** 2152–2169.

Lamb, R. G., 1982: Diffusion in the convective boundary layer. *Atmospheric Turbulence and Air Pollution Modeling,* F. T. M. Nieuwstadt and H. van Dop, Eds., Reidel, 159–229.

Lenschow, D. H., J. C. Wyngaard, and W. T. Pennell, 1980: Mean-field and second-moment budgets in a baroclinic, convective boundary layer. *J. Atmos. Sci.*, **37,** 1313–1326.

Luhar, A. K., and R. E. Britter, 1989: A random walk model for dispersion in inhomogeneous turbulence in a convective boundary layer. *Atmos. Environ.*, **23,** 1911–1924.

Mellor, G. L., and T. Yamada, 1974: A hierarchy of turbulence models for planetary boundary layers. *J. Atmos. Sci.*, **31,** 1791–1806.

——, and ——, 1982: Development of a turbulence closure model for geophysical fluid problems. *Rev. Geophys. Space Phys.*, **20,** 851–875.

Moeng, C.-H., 1984: A large-eddy simulation for the study of planetary boundary layer turbulence. *J. Atmos. Sci.*, **41,** 2052–2062.

——, and J. C. Wyngaard, 1984: Statistics of conservative scalars in the convective boundary layer. *J. Atmos. Sci.*, **41,** 3161–3169.

——, and ——, 1989: Evaluation of turbulent transport and dissipation closures in second-order modeling. *J. Atmos. Sci.*, **46,** 2311–2330.

Nieuwstadt, F. T. M., and J. P. J. M. de Valk, 1987: A large eddy simulation of buoyant and nonbuoyant plume dispersion in the atmospheric boundary layer. *Atmos. Environ.*, **21,** 2573–2587.

Quintarelli, F., 1990: A study of vertical velocity distributions in the planetary boundary layer. *Bound.-Layer Meteor.*, **52,** 209–219.

Reid, J. D., 1979: Markov chain simulations of vertical dispersion in the neutral surface layer for surface and elevated releases. *Bound.-Layer Meteor.*, **16,** 3–22.

Robinson, S. K., 1991: The kinematics of turbulent boundary layer structure. Ames Research Center, NASA Tech. Mem. 103859, 15–52.

Sawford, B. L., and F. M. Guest, 1987: Lagrangian stochastic analysis of flux-gradient relationships in the convective boundary layer. *J. Atmos. Sci.*, **44,** 1152–1165.

Schmidt, H., and U. Schumann, 1989: Coherent structure of the convective boundary layer derived from large-eddy simulations. *J. Fluid Mech.*, **200,** 511–562.

Scott, K., 1994: A comparison of predicted mean surface trace concentration for three models: Random walk, Gaussian and K-theory. M.S. thesis, Graduate Group in Atmospheric Science, University of California, Davis, 1–70.

Seibert, P., and B. Morariu, 1991: Improvement of upstream, semi-Lagrangian numerical advection schemes. *J. Appl. Meteor.*, **30,** 117–125.

Shaw, R. H., K. T. Paw U, and W. Gao, 1989: Detection of temperature ramps and flow structures at a deciduous forest site. *Agric. For. Meteor.*, **47,** 123–138.

Stull, R. B., 1988: *An Introduction to Boundary Layer Meteorology.* Kluwer Academic, 666 pp.

Thomson, D. J., 1987: Criteria for the selection of stochastic models of particle trajectories in turbulent flows. *J. Fluid Mech.*, **180,** 529–556.

Webb, E. K., 1964: Daytime thermal fluctuations in the lower atmosphere. *Appl. Opt.*, **3,** 1329–1336.

Weil, J. C., 1990: A diagnosis of the asymmetry in top-down and bottom-up diffusion using a Lagrangian stochastic model. *J. Atmos. Sci.*, **47,** 501–515.

Willis, G. E., and J. W. Deardorff, 1976: A laboratory model of diffusion into the convective boundary layer. *Quart. J. Roy. Meteor. Soc.*, **102,** 427–445.

——, and ——, 1978: A laboratory study of dispersion from an elevated source within a modeled convective planetary boundary layer. *Atmos. Environ.*, **12,** 1305–1311.

——, and ——, 1981: A laboratory study of dispersion from a source in the middle of the convective mixed layer. *Atmos. Environ.*, **15,** 109–117.